Journal of Materials Chemistry C

Accepted Manuscript

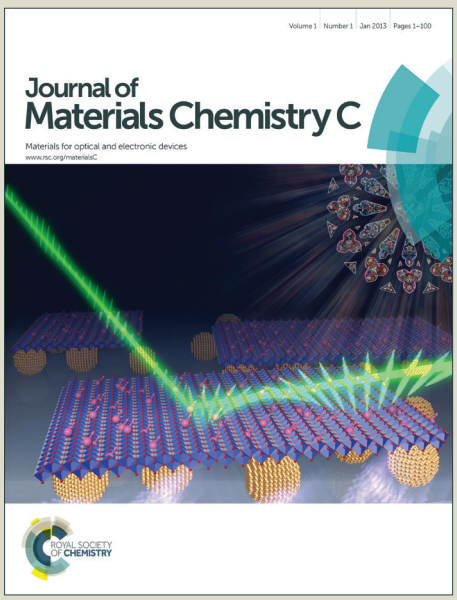

ROYAL SOCIETY OF CHEMISTRY

www.rsc.org/materialsC

Co-doped NiO nanoflake array films with enhanced electrochromic properties

Jia-heng Zhang [a], Guo-fa Cai [a], Ding Zhou [a], Hong Tang [a], Xiu-li Wang [a,b], Chang-dong Gu [a,b] and Jiang-ping Tu [a,b]*

a. State Key Laboratory of Silicon Materials, Key Laboratory of Advanced Materials and Applications for Batteries of Zhejiang Province and Department of Materials Science and Engineering, Zhejiang University, Hangzhou 310027, China

b. Cyrus Tang Center for Sensor Materials and Applications, Zhejiang University, Hangzhou 310027, China

*Corresponding Author

Tel.: +86 571 87952856. Fax: +86 571 87952573.

E-mail: tujp@zju.edu.cn; tujplab@zju.edu.cn (J.P. Tu)

Abstract

Co-doped NiO electrochromic nanoflake array films grown on FTO with antireflection ability have been synthesized by low temperature chemical bath deposition. Co doping has an influence on the growth and electrochromic properties of NiO nanoflake arrays. Noticeably, all the films show a very high transmittance at the bleached state in the region of visible light. Compared to the undoped NiO, the 1% Co-doped NiO nanoflake array film exhibits an outstanding electrochromism, including large transmittance modulation (88.3%), high coloration efficiency (47.7 cm^2 C^{-1}), fast switching speed (3.4 s and 5.4 s), excellent reversibility and cycling durability at a wavelength of 550 nm. The enhanced electrochromic performances can be attributed to the synergetic effect contribution from low crystallization, oblique nanoflake array configuration and improved p-type conductivity by appropriate Co doping.

1. Introduction

Electrochromism is a process by which the color of a material is changed reversibly and persistently through an electrochemical reaction. [1,2] Since the discovery of electrochromism, there have been intense research interests on electrochromic materials (ECs) due to their low power consumption, high coloration efficiency (*CE*), and stable memory effect under open circuit condition. Currently, they have been widely applied in various fields, such as energy-efficient glazing, large area displays, automobile sunroofs, military camouflage windows, smart mirrors, and so forth.[1–7]. Therefore, by function-oriented selection of practical application, the ECs with long-term cyclic stability, high coloration efficiency, large optical modulation and short switching time under a very low dc voltage are highly expected.

Several kinds of materials such as transition-metal oxides, mixed valence materials, conjugated polymers, and organic molecules have been reported to exhibit electrochromic properties.[8,9] Among the transition-metal oxides, NiO is an attractive anodic EC due to its high electrochromic efficiency, large dynamic range and low material cost.[10–13]. However, difficulties have been encountered in the commercial exploitation of NiO electrochromic film due to its slow switching speed, low color contrast and poor cycling durability. Recently, it was found that doping of other elements (Li, B, Cu, Al, Ni, Cs, W, etc.) to NiO films could enhance their optical properties and cyclability. [3,14–24] Both NiO and CoO have a cubic structure with lattice parameters 4.17 Å and 4.26 Å, and the low lattice mismatch (2.1%) between them is conducive to substitutional doping. Meanwhile, the similar ion radii of Ni and Co

would make it possible to dope NiO by Co without causing much lattice strain. Based on these considerations, Co has been considered a promising doping element for the NiO-based electrochromic film.

Up to now, numerous methods have been developed to fabricate NiO electrochromic films including sputtering,[25,26] electrodeposition,[27,28] sol–gel processing, [29,30] chemical vapor deposition,[31,32] pulsed laser deposition [33,34] spray pyrolysis, [35,36] hydrothermal method,[12,13] and chemical bath deposition (CBD) [37−39], *etc.* Among these methods, CBD is an advantageous technique due to its low cost, low temperature required and convenience for large-area deposition. Herein, we report a one-step method for producing Co-doped electrochromic NiO thin film on FTO-coated glass by CBD. The effects of Co doping on the microstructure and electrochromic performance of NiO films were investigated. It was found that the switching speed and cycling durability were significantly enhanced with appropriate Co doping in NiO. To the best of our knowledge, it is the first time to report Co-doped NiO nanoflake array film fabricated by CBD toward electrochromism.

2. Experimental

2.1 Chemical materials

All solvents and chemicals were of analytical grade and used without further purification. FTO-coated glass was purchased from Zhuhai Kaivo Electronic Components Co., Ltd. Nickel sulfate, cobalt sulfate, potassium persulfate and aqueous ammonia (25–28%) were obtained from Sinopharm Chemical Reagent Co., Ltd.

(China). All aqueous solutions were freshly prepared with de-ionized water.

2.2 Preparation of Co-doped NiO film

The synthetic routes of CBD for the Co-doped NiO nanoflake array films have been described detailedly in our previous reports. [37,39] Firstly, fluorine-doped tin oxide (FTO)-coated glass (4×2 cm^2 in size) was washed with acetone, ethanol and finally deionized water in an ultrasonic bath for 30 min. The back side of FTO was masked with polyimide tape to prevent the deposition on the nonconductive side. Solution for CBD was obtained by mixing 0.12 mol $NiSO_4$ and $CoSO_4$ (the atomic percentage of Co is 0.3%, 0.5%, 1% and 3%), 0.0225 mol potassium persulfate, 30 ml of aqueous ammonia (25–28%) and 270 ml de-ionized water in a 500 ml pyrex at 30 ºC. The FTO substrates, placed vertically in the freshly resulting solution, were kept at 30 ºC for 6 min to deposit the precursor films. For comparison, pure NiO film was also prepared with the same processes without the addition of $CoSO_4$. After removing the tape masks, the precursor films were rinsed with distilled water and then annealed in a tube furnace at 350 ºC for 2 h in flowing argon after drying. However, it should be noted that the so-called doping amounts are nominal compositions of cobalt, based on the atomic percentage of Co with respect to Ni in the initial reagents. The as-prepared films were denoted as NiO (for undoped NiO), NiO-Co 0.3, NiO-Co 0.5, NiO-Co 1, NiO-Co 3, respectively.

The microstructure and surface morphology of the as-prepared films were analyzed using X-ray diffraction (XRD, RIGAKU D/MAX 2550/PC with Cu Kαradiation), X-ray photoelectron spectroscopy (XPS, AXIS UTLTRADLD equipped

with a dual Mg Ka-Al Kaanode for photoexcitation), field emission scanning electron microscopy (FESEM, Hitachi SU-70),high-resolution transmission electron microscopy (HRTEM, Tecnai F20) and inductively coupled plasma mass spectrometry (ICP-MS, Xeries II).

2.3 Electrochemical measurements

Cyclic voltammetry (CV) and chronoamperometry (CA) measurements were carried out on a CHI660 Eelectrochemical workstation in a three-electrode electrochemical cell, with 1 MKOH as the electrolyte, platinum foil as the counter electrode and Hg/HgO as the reference electrode. The CV tests of the NiO films were performed at a scan rate of 20 mV s^{-1} between −0.2 and 0.8 V at room temperature (20 ± 1 ºC). Electrochemical impedance spectrum (EIS) tests were conducted on this electrochemical workstation with a superimposed 5 mV sinusoidal voltage in the frequency range of 0.01 Hz−100 kHz. The transmittance spectra of the films in the fully colored and fully bleached states were measured over the wavelength range from 300 to 1000 nm with a SHIMADZU UV-3600 spectrophotometer. The refractive index measurement from 357 to 800 nm was carried out by a GES5E spectroscopic ellipsometer with Cauchy and Drude models. Raman spectra were recorded on LABRAM HR-800 at an excitation wavelength of 514 nm, and the FTIR spectra were conducted by Nicolet 5700.

3. Results and discussion

3.1. Structure and Morphology

The XRD patterns of the powders scratched from the as-prepared films on FTO substrate are presented in Fig. 1. The diffraction peaks in all the patterns are corresponding to a cubic NiO phase (JCPDS No. 73-1523). There are no extra peaks detectable for cobalt oxides or other impurities, implying that Co doping does not change the original NiO structure. The patterns show no detectable peak shift, which indicates a substitutional doping. Nevertheless, the diffraction peaks of the Co-doped NiO films broaden as the doping content increases, indicating that the grain size of Co-doped NiO is smaller, or lower crystallinity of them. The metal stoichiometries of the doped films are shown in Table 1. There are some differences in metal stoichiometry between the precursor solutions and as-prepared films. When the content of cobalt is low in the precursor solution, the NiO lattices would tend to accept the addition of cobalt from the solution. Hence, the content of cobalt in the films is a little higher than the precursor solution. With the increase of cobalt in solution, the cobalt capacity of NiO lattices might have reached saturation below 3%. Therefore, the cobalt of NiO-Co3 is less than 3%.

In order to study the surface compositions and chemical states of the NiO films, we conducted XPS analysis in the present work. The full survey spectrum of NiO-Co1 film is shown in Fig. 2a. The Co 2p characteristic peaks of CoO are detected in the inset of Fig. 2a, indicating the existence of CoO in the Co-doped NiO films.[23, 40, 41] The 3/2 spin-orbit components of Ni 2p ionization region for the NiO and NiO-Co1 films are shown in Fig. 2b. The Ni $2p_{3/2}$ signals can be deconvoluted into three peaks, peak A, B and C corresponding to Ni^{2+}, Ni^{3+} and satellite structure, respectively. The

Ni^{3+} mainly derives from high valence nickel oxides such as $Ni_2O_3 \cdot H_2O$, β-NiO(OH), or $4Ni(OH)_2 \cdot NiOOH \cdot xH_2O$ due to the effect of persulfate.[42] The positions of these peaks are almost the same for NiO and NiO-Co1 films, however, the intensity ratio of peak A/peak B decreases obviously after Co doping. According to the previous work,[43] pure NiO flim is a n-type semiconductor because of the presence of Ni^{3+}. After Co doping, Co^{2+} partially substitutes Ni^{3+}, leading to the increase of holes concentration. Then the enhanced p-type conductivity was obtained.[39,43] It is very useful to reduce the charge transfer resistance during the electrochromic process. The O1s spectra of NiO and NiO-Co1films are displayed in Fig. 2c. The O1s peaks of both the films mainly include two components, peak D and peak E corresponding to NiO and Ni-OH bands, respectively. The positions of the peaks in NiO-Co1 film are close to those of NiO, with a little shift due to the oxygen vacancy on the surface. Furthermore, there is one more O1s peak located at 529.6 eV in the spectrum of NiO-Co1 film, well corresponding to that observed for CoO. [44] Meanwhile, the intensity ratio of peak E / peak D decreases because of Ni^{3+} partially replaced by Co^{2+}, which is in accordance with the analysis of Ni $2p_{3/2}$ spectra. With the enhanced p-type conductivity, it is plausible that the Co-doped NiO nanoflake array films should have excellent electrochromic performance.

The surface and cross-sectional SEM images of the NiO films with and without Co doping are illustrated in Fig. 3. Except for NiO-Co3, all the films are uniform in appearance, exhibiting a porous and neck-connected structure (Fig. 3a-e). These films are made up of NiO nanoflakes with the similar thicknesses of 7−9 nm (Fig. 3b).

However, with the increase of Co doping, the thickness of the film become thin and the pore diameter among the nanoflakes decreases (Fig. 3c-f, inset). Interestingly, it is found that it cannot form a uniform nanoflake array when the amount of doped Co reaches 3 % (Fig. 3f). Obviously, the addition of $CoSO_4$ in the CBD solution exerts an effect on the growth of NiO film. This phenomenon can be explained that $CoSO_4$ inhibits the transition from β-$Ni(OH)_2$ to γ-NiOOH,[45] while γ-NiOOH with a higher valence stateis conducive to the growth of NiO film.[39] In addition, the electrochemically accessible surface area of NiO film with appropriate amount Co doping should be greater than that of undoped NiO film because of the existence of small pores. The high specific area coupled with nanoporosity will make it easy for electrolyte penetration, which is helpful for the improvement in electrochromic performances.

The HRTEM images shown in Fig. 4 reveal distinct differences of detailed microstructure between the undoped and Co-doped NiO films. The NiO film exhibits a porous and well-crystalline interconnected-like architecture (Fig. 4a), with a lattice spacing of about 0.210 nm corresponding to the (200) plane of NiO (Fig. 4b). With the increase of Co-doped amount, the wrinkles (nanoflakes) become denser and vaguer until approximate disappearing (Fig. 4c and e). At the same time, the lattice spacing corresponding to the (200) plane enlarges (Fig. 4d and f). It can be attributed to the fact that the Ni ions are replaced by Co ions with large radius, and the consequent stretcher strain among the lattice results in an increase of the lattice parameters.

3.2. Electrochemical and Electrochromic Performances

To compare the electrochemical and electrochromic performances accurately, we deliberately adjust the deposition time to obtain a similar thickness (about 250 nm) of the NiO films. The electrochromic performances of the NiO films are evaluated using CV measurements. Fig. 5 compares the CV curves of undoped and Co-doped NiO films carried out in 1 M KOH solution with the potential region of −0.2− 0.8 V at a scan rate of 20 mV s^{-1} for the 10th cycle. Only one pair of redox peaks is observed for all the films. The anodic/cathodic peaks are assigned to the conversion between NiO and NiOOH due to OH^- insertion/desertion. As the OH^- ions inserting and deserting, the films are colored and bleached reversibly because of the transformation between Ni^{3+} and Ni^{2+}. The involved reactions can be simply illustrated as $NiO + OH^- \leftrightarrow NiOOH + e^-$. In order to support that electronic change results in the coloration, the XRD and XPS of the NiO and NiO-Co1 films in the colored state (0.8 V) were conducted. The XRD patterns are shown in the Fig. 7a. The characteristic peaks corresponding to NiOOH (JCPDS 06-00075) can be observed, as well as NiO. The XRD patterns confirm that most NiO changes into NiOOH in the coloration for both the films, which is consistent with the proposed reaction in CV analysis. No obvious difference can be observed between the two films. For the Ni $2p_{3/2}$ XPS spectra (Fig. 6a), the intensity ratio of peak B / peak C for both the films increases obviously after coloration, which support the transformation from NiO to NiOOH. What's more, the intensity ratio of NiO-Co1 film increases more obviously, indicating more NiOOH formation. The same result can be observed from the O 1s spectra, shown in Fig. 6b,

indicating that the proposed reaction mechanism is reasonable. What is noteworthy, with the increase of Co doping amount, the potential separation between the oxidation and reduction peaks becomes much narrow, revealing weak polarization and good reversibility. Meanwhile, the high peak currents and large integral areas of the Co-doped NiO films are observed. It indicates that Co doping affects the ionic and electronic conductivity of the active material, leading to a high electrode utilization and improvement of reaction kinetics.[46] Nevertheless, the cathodic and anodic peaks become low when the Co doping amount increases to 3%. As shown in Fig. 2f, NiO-Co3 exhibits small pores. It is well known that the large specific surface area can shorten the path of ionic diffusion, however, the undersized pores may make it difficult for the electrolyte to infiltrate. On the other hand, when the amount of doped Co is excessive, part of the Co dopant could not enter the lattice structure of NiO but constituted an impurity, which might hinder the ionic transfer and diffusion in return.[47] No obvious electrochemical current peaks corresponding to Co can be observed in the potential range, indicating that the amount of cobalt is too small to be detected or it has not participated in reaction. The above findings imply that the optimum Co doping in NiO film for the OH^- insertion reaction is 1 %.

In order to further verify the formation of NiOOH, the Raman and FTIR spectra of NiO-Co1 in both bleached and colored states were conducted. Fig. 7a shows the Raman spectra of the NiO-Co1 film. For the bleached film, a broad band centered at 550 cm^{-1} can be observed, which is attributable to NiO.[7, 48] Then the film is cycled by applying a step voltage of 0.8 V to reach the colored state. The characteristic spectrum

of NiOOH is obtained, exhibiting a Raman profile with a couple of strong bands at 473 and 555 cm^{-1} attributed to stretching vibrational modes involving [Ni^{3+}=O] and [Ni^{3+}–O] sites, respectively. [49] The FTIR spectra of powders of the NiO-Co1 film from FTO substrate are shown in Fig. 7b. A decrease in NiO after coloration can be observed from the decrease in Ni–O stretching vibrational mode at 465 cm^{-1} and the transversal optical vibration mode of the $Ni(OH)_2$ at 436 cm^{-1}. That can be seen together with the increase of NiOOH due to the υ (Ni^{3+}–O) bending vibration mode at about 600 cm^{-1}. [50] From the above experimental results, we can come to the conclusion that the film was colored with the formation of NiOOH.

The optical transmittance measurements are conducive to analysis the stability, reversibility and switching response of the NiO films. The transmittance spectra in the colored and bleached states from 300 nm to 1000 nm are presented in Fig. 8a, which are measured after the film electrodes subjected to CV test for 10 cycles in 1 M KOH solution. As seen in this figure, Co doping leads to a significant decrease in transmittance of NiO film at the colored state, whereas the transmittance at bleached state decreases by a large margin when the amount of Co doping reaches 3%. It can be ascribed to the increase of Ni oxidation states resulting from Co acting as a p-type dopant.[51] On the other hand, based on the reversible reaction $NiO + OH^- \leftrightarrow NiOOH + e^-$ and Le Chatelier's principle, the reaction tends to form NiOOH when partly Ni^{3+} is replaced by the doped Co^{2+}. The phenomenon is in accordance with the report by Purushothaman et al.[24] The modulation ranges of transmittance for the undoped and Co-doped NiO films at 550 nm are given in Table 1. Herein, the transmittance

variation of NiO film exhibits about 71.5 % at 550 nm, while NiO-Co0.5 and NiO-Co1 reaches about 89.3% and 88.3% respectively, which is larger than most of NiO electrochromic films in previously reportedworks.[12,38,52−54] Interestingly, it is surprised to find that the transmittances of certain spectral regions at bleached state exceed 100 %. No report has described this phenomenon about NiO film in visible light region. However, many similar phenomena were reported for other transitional metal oxide films, such as TiO_2 and Ta_2O_5.[55−57] The increased optical transparency can be attributed to the antireflection. In order to prove the ability of antireflection for the as-prepared films, the refractive index measurement of NiO-Co1 film was carried out as an example. According to the relationship $n_f = (n_0 n_s)^{1/2}$ (n_f, n_0 and n_f are the refractive indices of the antireflection layer, air and the substrate, respectively), and the refractive index of FTO grass is closer to 1.5− 2.0,[58,59] the value of n_f should be 1.2−1.4 on FTO. As shown in Fig. 8b, the refractive index of NiO-Co1 film is 1.39 at a wavelength of 550 nm. The above fact can well prove the increased optical transparency resulting from the antireflection ability, which may be induced by the NiO nanoflakes. The obliquely standing and porous structures are the key to effectively reduce the refractive index.[59−61] The photographs of NiO-Co1 film at bleached and colored states are shown in Fig. 9a and 9b. Meanwhile, bare FTO substrate is slightly white due to scattering of visible light by rough surface (Fig. 9c, the top of the grass), but the FTO substrate covered with NiO film shows high transparency.

With such promising results, we further investigate the switching times of the

films by CA and the corresponding transmittance in situ at 550 nm, as shown in Fig. 10a and b. The switching time is defined as the duration to reach 90% of its full modulation. The coloration and bleaching times of all the films are listed in Table 1. NiO-Co1 film reveals the fastest coloration and bleaching times for 5.4 s and 3.4 s respectively, while the NiO film needs 8.8 s and 4.4 s. Moreover, the switching times of NiO-Co1 film are faster than those NiO films prepared by chemical precipitation (5.8 s and 4.4 s), [2] electrodeposition (6 s and 10 s),[54] radio frequency magnetron sputtering (18.7 s and 14.5 s), [20] and spray pyrolysis (15 s and 20 s). [62] The fast switching speed of NiO-Co1 film is attributed to the synergetic effect contribution from the low crystallization, nanoflake array configuration, and enhanced electronic conductivity after Co doping, which is coincident with the result of CV measurements. Hence, it can be concluded that appropriate Co doping can enhance the switching speed of NiO electrochromic film prepared by CBD.

CE is a useful figure of merit for the comparison of various electrochromic materials, which is evaluated through the following equations:

$$CE(\lambda)=\frac{\Delta OD(\lambda)}{Q} \quad (1)$$

$$\Delta OD(\lambda)=\log\frac{T_b}{T_c} \quad (2)$$

$$Q=\int_{t1}^{t2} j(t)dt \quad (3)$$

where ΔOD is the chance in optical density at a wavelength, depending on the transmittances in the bleached (T_b) and colored (T_c) states; Q is the inserted(or extracted) charge during the coloring period. An ideal EC should maximize its *CE*,

corresponding to a large modulation range of transmittance induced by a small amount of charge.[63] The calculated values of *CE* for the NiO films are listed in Table 1. NiO-Co1 film exhibits an optimum *CE* value, as high as 47.69 cm^2 C^{-1}. The enhanced *CE* value is a direct consequence of Co doping, which combines a high specific surface area providing good ion access and a large modulation range of transmittance with a high electric conductivity.

In order to further prove that the NiO film with appropriate Co doping has an enhanced electric conductivity, the EIS and sheet resistance are measured on NiO and NiO-Co1 films. Fig. 11 shows the EIS plots after the film electrodes had been subjected to CV test for 10 cycles. The Nyquist plots of both films are constituted by a single depressed semicircle in the high frequency region and an inclined line at low frequency region. Generally, the semicircle reflects the electrochemical reaction impedance of the film electrode and the line reflects the diffusion of the electroactive species. The elements in the equivalent circuit (see inset in Fig. 11) include ohmic resistance (R_s), which is a combinational resistance of electrolyte resistance, intrinsic resistance of substrate, and contact resistance at the active material/current collector interface, [64] charge-transfer resistance (R_{ct}) caused by the Faradaic reaction, the capacitance of the double layer (Q_c), and Warburg impedance (W). These parameters are calculated through the plots with ZView software and listed in Table 2. The value of Q_c of the NiO-Co1 film is lower than that of the NiO film. It can be inferred that the NiO-Co1 film has larger reaction surface. Meanwhile, the semicircle for the NiO-Co1 film in the high frequency range is smaller than that of the NiO film. A

smaller semicircle means a smaller charge-transfer resistance and the calculated R_{ct} for the NiO-Co1 and NiO films are 9.75 and 12.03 Ω, respectively. Additionally, the low-frequency tail represents Warburg impedance related to ion diffusion between electrolyte and electrode, and the higher slope of inclined line in the high frequency range means the lower diffusion rate.[38] Compared to the NiO film, the lower slope of inclined line for the NiO-Co1 film signifies a higher ion-diffusion rate. What' more, the NiO-Co1 film has a smaller sheet resistance (R_{sr}) than the NiO film, as shown in Table 2. The above results amply demonstrate that the appropriate Co doping can enhance electric conductivity of NiO film.

As we know, the electrochromic NiO film prepared by CBD has a poor cycling durability, whereas, the cycling stability can be a concern for the practical application of ECs. Herein, an evaluation of the cycling durability for the NiO and NiO-Co1 film electrodes was performed with a 3000-cycle test (Fig. 12a). Noticeably, the improved cycling durability at 550 nm and enhanced color contrast of NiO-Co1 film can be observed comparing with NiO film. After subjected for 900 cycles, the modulation ranges of transmittance decayed for about 35.4% and 94.4% for NiO-Co1 and NiO films, respectively. Furthermore, even subjected to 3000 cycles, the transmittance modulation of NiO-Co1 film decayed only for 54.0%. The SEM images of the NiO and NiO-Co1 films after 1000 cycles are illustrated in Fig. 12b and 12c. The nanoflakes become very thin and a large number of active material fell off the NiO film electrode. However, there is nearly no change with the NiO-Co1 film after 1000 cycles except for the nanoflakes being a little thinner, which also proves the excellent

cycling durability. The cycling durability of NiO-Co1 film is more excellent than those NiO films reported by Cai *et al* (sustaining 40% after 600 cycles),[7] Xia *et al* (sustaining 40% after 300 cycles),[37] and Purushothaman *et al* (remaining 42% at 1210th cycle).[65] The degradation mechanism of NiO film for electrochromism in alkaline medium is associated with structure disintegration, which mainly caused by volumetric change during the continuous conversion of NiO ↔ NiOOH, and oxygen bubbles striking generated from the accompanying oxygen evolution reaction (OER) for NiO film electrode in alkaline aqueous solution.[66, 67] The enhanced cycling durability of the NiO film with appropriate Co doped can be possibly attributed to the following reasons. First, during the electrochromic reaction, the doped cobalt ions in the NiO lattice could play the role of the buffer for volumetric change. Second, the unique nanoflake array architecture can reduce internal strain and accommodate the vast volume changes.[67, 68] Last, the improved electronic conductivity of Co doping NiO film can maximize the effective electrochemical utilization of the active materials and ensure a reversible OH^- insertion/extraction process even at high current rates.[69] The interaction of all these factors leads to slow degradation and better cycling stability.

4. Conclusions

Co-doped NiO nanoflake array electrochromic films with antireflection ability grown on FTO have been synthesized by CBD method. Co doping significantly affects the growth of NiO film during CBD process. Compared to the undoped NiO film, the advisable Co-doped (1%) NiO film exhibits excellent electrochromic performances,

such as large transmittance modulation, fast switching speed, high coloration efficiency and good cycling durability. These enhanced electrochromic performances can be attributed to the synergetic effect contribution from low crystallization, oblique nanoflake array configuration and improved electronic conductivity by appropriate doping of Co. In view of the noticeable fast switching speed, enhanced reversibility and cycling durability, it is appreciable that Co doping can promote the commercialization of NiO based electrochromic film.

Acknowledgments

This work was supported by the Program for Innovative Research Team in University of Ministry of Education of China (IRT13037), Key Science and Technology Innovation Team of Zhejiang Province (2010R50013) and a support program of the Ministry of Education of China.

References

1. I. Y. Cha, S. H. Park, J. W. Lim, S. J. Yoo and Y. E. Sung, *Solar Energy Mater. Solar Cells*, 2013, **108**, 22.
2. D. S. Dalavi, R. S. Devan, R. S. Patil, Y. R. Ma, M. G. Kang, J. H. Kim and P. S. Patil, *J. Mater. Chem. A*, 2013, **1**, 1035.
3. H. Moulki, D. H. Park, B. K. Min, H. Kwon, S. J. Hwang, J. H. Choy, T. Toupance, G. Campet and A. Rougier, *Electrochim. Acta*, 2012, **74**, 46.
4. B. Kattouf, Y. Ein-Eli, A. Siegmann and G. L. Frey, *J. Mater. Chem. C*, 2013, **1**, 151.
5. C. G. Granqvist, *J. Eur. Ceram. Soc.*, 2005, **25**, 2907.
6. J. Zhang, X. L. Wang, X. H. Xia, C. D. Gu and J. P. Tu, *Solar Energy Mater. Solar Cells*, 2011, **95**, 2107.
7. G. F. Cai, J. P. Tu, C. D. Gu, J. H. Zhang, J. Chen, D. Zhou, S. J. Shi and X. L. Wang, *J. Mater. Chem. A*, 2013, **1**, 4286.
8. J. Matsui, R. Kikuchi and T. Miyashita, *J. Am.Chem. Soc.*, 2013**,136**, 842.
9. M. V. Nguyen, D. Kim and H. Kim, *J. Mater. Chem. C*, 2013, **1**, 3399.
10. S. Pereira, A. Gonçalves, N. Correia, J. Pinto, L. Pereira, R. Martins and E. Fortunato, *Solar Energy Mater. Solar Cells*, 2014, **120**,109.
11. G. A. Niklasson and C. G. Granqvist, *J. Mater. Chem.*, 2007, **17**, 127.
12. F. Cao, G. X. Pan, X. H. Xia, P. S. Tang and H. F. Chen, *Electrochim. Acta*, 2013, **111**, 86.
13. J. Y. Liu, Y. Ren, B. Dasgupta, H. Tanoto, H. L. Seng, W. K. Chim, S. F. Y. Li and S. Y. Chiam, *J. Mater. Chem. A*, 2013, **1**, 15095.
14. I. A. Garduño, J. C. Alonso, M. Bizarro, R. Ortega, L. Rodríguez-Fernández and A. Ortiz, *J. Cryst. Growth*, 2010, **312**, 3276.
15. R. C. Tenent, D. T. Gillaspie, A. Miedaner, P. A. Parilla, C. J. Curtis and A. C. Dillon, *J. Electrochem. Soc.*, 2010, **157**, H318.
16. H. Aydin, S. A. Mansour, C. Aydin, A. Al-Ghamdi, O. Al-Hartomy, F. El-Tantawy and F. Yakuphanoglu, *J. Sol-Gel Sci. Technol.*, 2012, **64**, 728.
17. X. C. Lou, X. J. Zhao, J. M. Feng and X. D. Zhou, *Prog. Org. Coat.*, 2009, **64**, 300.

18. X. C. Lou, X. J. Zhao and X. He, *Solar Energy*, 2009, **83**, 2103.
19. L. L. Zhao, G. Su, W. Liu, L. X. Cao, J. Wang, Z. Dong and M. Q. Song, *Appl. Surf. Sci.*, 2011, **257**, 3974.
20. F. Lin, D. T. Gillaspie, A. C. Dillon, R. M. Richards and C. Engtrakul, *Thin Solid Films*, 2013, **527**, 26.
21. F. A. Al-Agel, *Mater. Lett.*, 2013, **100**, 115.
22. N. Penin, A. Rougier, L. Laffont, P. Poizot and J. M. Tarascon, *Solar Energy Mater. Solar Cells.*, 2006, **90**, 422.
23. Z. Zheng, L. Huang, Y. Zhou, X. W. Hu and X. M. Ni, *Solid State Sci.*, 2009, **11**, 1439.
24. K. K. Purushothaman and G. Muralidharan, *J. Non-Cryst. Solids*, 2012, **358**, 354.
25. B. Subramanian, M. Mohamed Ibrahim, V. Senthilkumar, K. R. Murali, V. S. Vidhya, C. Sanjeeviraja and M. Jayachandran, *Physica B*, 2008, **403**, 4104.
26. E. L. Miller and R. E. Rocheleau, *J. Electrochem. Soc.*,1997, **144**, 1995.
27. G. Su, M. Q. Song, W. Z. Sun, L. X. Cao, W. Liu, D. W. Ma, N. Chen, L. L. Zhao, J. Wang and X. Y. Liu, *Sci. China Technol. Sci.*, 2012, **55**, 1545.
28. D. S. Dalavi, M. J. Suryavanshi, S. S. Mali, D. S. Patil and P. S. Patil, *J. Solid State Electrochem.*, 2012, **16** , 253.
29. K. K. Purushothaman, S. Joseph Antony and G. Muralidharan, *Solar Energy*, 2011, **85**, 978.
30. A. Šurca, B. Orel, B. Pihlar and P. Bukovec, *J. Electroanal. Chem.*, 1996, **408**, 83.
31. M. Z. Sialvi, R. J. Mortimer, G. D. Wilcox, A. M. Teridi, T. S. Varley, K. G. U. Wijayantha and C. A. Kirk, *ACS Appl. Mater. Interfaces*, 2013, **5**, 5675.
32. T. Maruyama and S. Arai, *Solar Energy Mater. Solar Cells*,1993, **30**, 257.
33. I. Bouessay, A. Rougier and J.M. Tarascon, *J. Electrochem. Soc.*, 2004, **151**, H145.
34. Y. Makimura, A. Rougier and J.M. Tarascon, *Appl. Surf. Sci.*, 2006, **252**, 4593.
35. B. A. Reguig, A. Khelil, L. Cattin, M. Morsli and J. C. Bernède, *Appl. Surf. Sci.*, 2007, **253**, 4330.
36. U. Alver, H. Yaykaşlı, S. Kerli and A. Tanrıverdi, *Int. J. Miner Metall. Mater.*, 2013, **20**, 1097.
37. X. H. Xia, J. P. Tu, J. Zhang, X. L. Wang, W. K. Zhang and H. Huang, *Solar Energy*

Mater. Solar Cells, 2008, **92**, 628.

38. X. H. Xia, J. P. Tu, J. Zhang, X. L. Wang, W. K. Zhang and H. Huang, *Electrochim. Acta*, 2008, **53**, 5721.
39. Y. J. Mai, J. P. Tu, X. H. Xia, C. D. Gu and X. L. Wang, *J. Power Sources*, 2011, **196**, 6388.
40. S. C. Petitto, E. M. Marsh, G. A. Carson and M. A. Langell, *J. Mol. Catal. A-Chem.*, 2008, **281**, 49.
41. G. A. Carson, M. H. Nassir and M. A. Langell, *J. Vac. Sci. Technol. A*, 1996, **14**, 1637.
42. S.Y. Han, D.H. Lee, Y.J. Chang, S.O. Ryu, T.J. Lee and C.H. Chang, *J. Electrochem. Soc.*, 2006, **153**, C382.
43. T. Dutta, P. Gupta, A. Gupta and J. Narayan, *J. Appl. Phys.*, 2010, **108**, 083715.
44. H. A. E. Hagelin-Weaver, G. B. Hoflund, D. M. Minahan and G. N. Salaita, *Appl. Surf. Sci.*, 2004, **235**, 420.
45. B. B. Ezhov and O. G. Malandin, *J. Electrochem. Soc.*, 1991, **138**, 885.
46. A. B. Yuan, S. A. Cheng, J. Q. Zhang and C. N. Cao, *J. Power Sources*, 1999, **77**, 178.
47. X. Li, S. H. Tang, M. Z. Qu, P. X. Huang, W. Li and Z. L. Yu, *J. Alloys Compd.*, 2014, **588**, 17.
48. G. Zhou, D. W. Wang, L. C. Yin, N. Li, F. Li and H. M. Cheng, *ACS Nano*, 2012, **6**, 3214.
49. S. Deabate, F. Fourgeot and F. Henn, *Electrochim. Acta*, 2006, **51**, 5430.
50. Y. Ren, W. K. Chim, L. Guo, H. Tanoto, J. Pan and S. Y. Chiam, *Solar Energy Mater. Solar Cells*, 2013, **116**, 83.
51. F. Lin, D. Nordlund, T. C. Weng, R. G. Moore, D. T. Gillaspie, A. C. Dillon, R. M. Richards and C. Engtrakul, *ACS Appl. Mater. Interfaces*, 2012, **5**, 301.
52. G. F. Cai, C. D. Gu, J. Zhang, P. C. Liu, X. L. Wang, Y. H. You and J. P. Tu, *Electrochim.Acta*, 2013, **87**, 341.
53. D. Y. Ma, G. Y. Shi, H. Z. Wang, Q. H. Zhang and Y. G. Li, *Nanoscale*, 2013, **5**, 4808.
54. Y. F. Yuan, X. H. Xia, J. B. Wu, Y. B. Chen, J. L. Yang and S. Y. Guo, *Electrochim. Acta*, 2011, **56**, 1208.
55. V. M. Aroutiounian, K. R. Maroutyan, A. L. Zatikyan and K. J. Touryan, *Thin Solid*

Films, 2002, **403–404**, 517.

56. Q. Z. Qin and Z. W. Fu, *Adv. Mater.*, 1999, **11**, 1119.
57. R. E. Thomas, S. Varma, D. Waechter, C. X. Dodd and S. R. Das, *Can. J. Phys.*, 1989**,** **67**, 430.
58. B. Stjerna, E. Olsson and C. G. Granqvist, *J. Appl. Phys.,* 1994, **76**, 3797.
59. J. Z. Chen, W. Y. Ko, Y. C. Yen, P. H. Chen and K. J. Lin, *ACS Nano*, 2012, **6**, 6633.
60. Y. Masuda and K. Kato, *J. Cryst. Growth*, 2009, **311**, 436.
61. J. Q. Xi, M. F. Schubert, J. K. Kim, E. F. Schubert, M. Chen, S. Y. Lin, W. Liu and J. A. Smart, *Nat.Photon.*, 2007, **1**, 176.
62. L. D. Kadam and P. S. Patil, *Solar Energy Mater. Solar Cells*, 2001, **69**, 361.
63. M. R. J. Scherer and U. Steiner, *Nano Lett.*, 2012, **13**, 3005.
64. M. L. Huang, C. D. Gu, X. Ge, X. L. Wang and J. P. Tu, *J. Power Sources*, 2014, **259**, 98.
65. K. K. Purushothaman and G. Muralidharan, *Mater. Sci. Semicond. Process.*, 2011, 14, 78.
66. N. Spinner and W. E. Mustain, *Electrochim. Acta*, 2011, **56**, 5656.
67. X. H. Xia, J. P. Tu, X. L. Wang, C. D. Gu and X. B. Zhao, *J. Mater. Chem*., 2011, **21**, 671.
68. Y. Gu, F. Wu and Y. Wang, *Adv. Funct. Mater.*, 2013, **23**, 893.
69. B. Liu, P. Soares, C. Checkles, Y. Zhao and G. Yu, *Nano Lett.,* 2013, 1**3**, 3414.

Table caption

Table 1 Electrochromic performances and metal stoichiometries of NiO films with different Co dopant.

Table 2 EIS parameters and sheet resistances of NiO and NiO-Co1 film electrodes in bleached state at 10th cycle.

Table 1

Film	Co/(Co+Ni) (at.%)-ICP	Modulation range of transmittance (%) at 500 nm	Switching speed (s)		Coloration efficiency ($cm^2\ C^{-1}$)
			t_b	t_c	
NiO	–	71.48	4.4	8.8	27.47
NiO-Co0.3	0.397	73.36	4.2	7.6	35.36
NiO-Co0.5	0.627	89.27	4.0	5.6	39.89
NiO-Co1	1.167	88.31	3.4	5.4	47.69
NiO-Co3	1.528	88.03	4.8	7.6	39.84

Table2

Film	R_s (Ω)	R_{ct} (Ω)	Q_c (μF)	R_w (Ω)	R_{sr} (Ω / sq)
NiO	3.01	12.03	0.19	15.23	10.41
NiO-Co1	2.50	9.75	0.24	11.03	8.46

Figure captions

Fig. 1 XRD patterns of undoped and Co-doped NiO nanoflakes.

Fig. 2 (a) XPS wide spectrum of NiO-Co1 film, the inset is Co 2p spectrum; (b) Ni $2p_{3/2}$ XPS spectra and (c) O 1s XPS spectra of NiO and NiO-Co1 films.

Fig. 3 SEM images of the films: (a, b) NiO, (c) NiO-Co0.3, (d) NiO-Co0.5, (e) NiO-Co1 and (f) NiO-Co3 (cross sectional view presented in inset)

Fig. 4 TEM images of (a, b) NiO, (c, d) NiO-Co1, and (e, f) NiO-Co3 films (inset corresponding SAED pattern).

Fig. 5 The 10th CV curves of the NiO films at a scan rate of 20 mV s^{-1}.

Fig. 6 (a) XRD patterns, (b) Ni 2p3/2 XPS spectra and (c) O 1s XPS spectra of NiO and NiO-Co1 films in the colored states.

Fig. 7 (a) Raman and (b) FTIR spectra of Ni-Co1film in both bleached and colored states.

Fig. 8 (a) Optical transmittance spectra of the NiO films at a wavelength of 550 nm (colored and bleached states), (b) refractive index curves for NiO-Co1 nanoflake array film from 375 to 800 nm.

Fig. 9 Photographs of NiO-Co1 film with a size of 4×2 cm^2 in (a) bleached state, (b) colored states, (c) the difference of transparency between the bare FTO area (top of a substrate) and Co-doped NiO film area.

Fig. 10 (a) CA with voltage interval from −0.2 V to 0.8 V, and (b) the corresponding transmittance in situ of the NiO films at 550 nm.

Fig. 11 Nyquist plots of NiO and NiO-Co1 film electrodes, and the equivalent

electrical circuit (inset) used to fit the experimental impedance spectra. Symbols denote experimental data, while the continuous lines represent the fitted data.

Fig. 12 (a) Durability tests of NiO and NiO-Co1 nanoflake array films for 3000 cycles at 550 nm; (b) SEM images of NiO and (c) NiO-Co1 films after 1000 cycles.

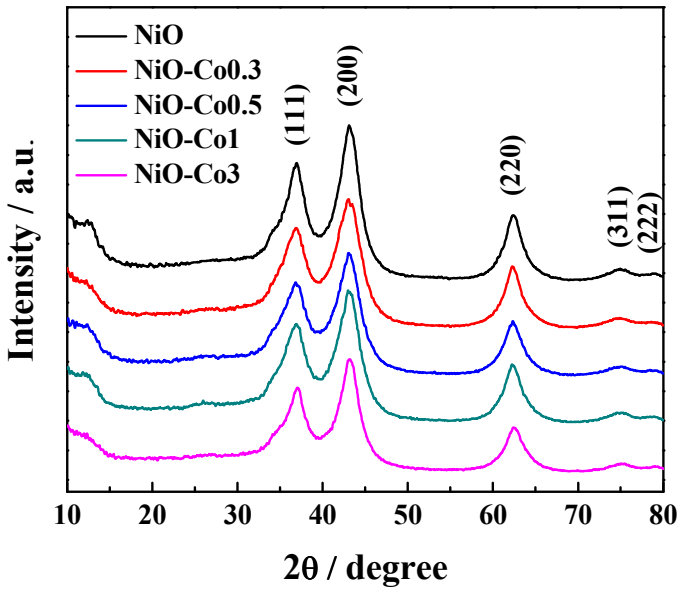

Fig. 1

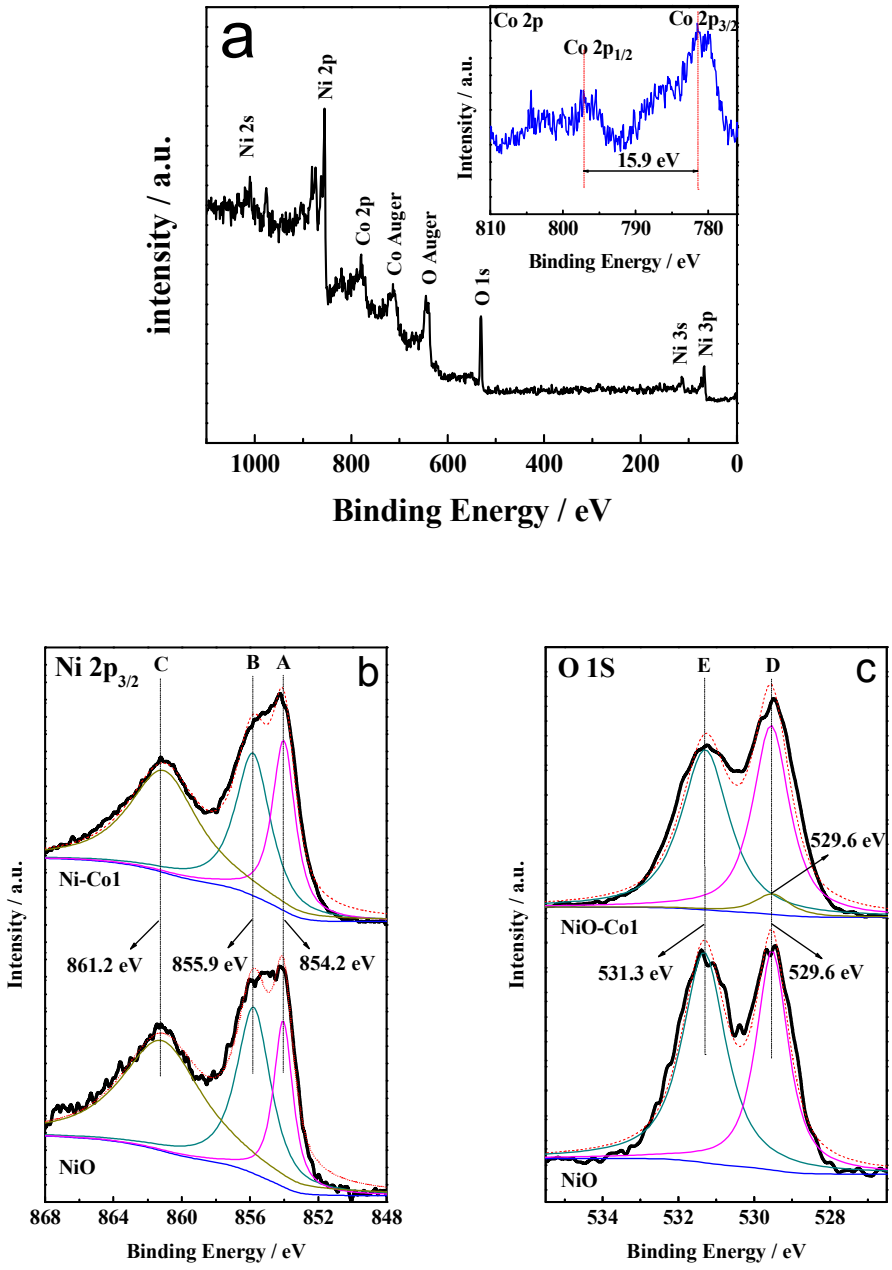

Fig. 2

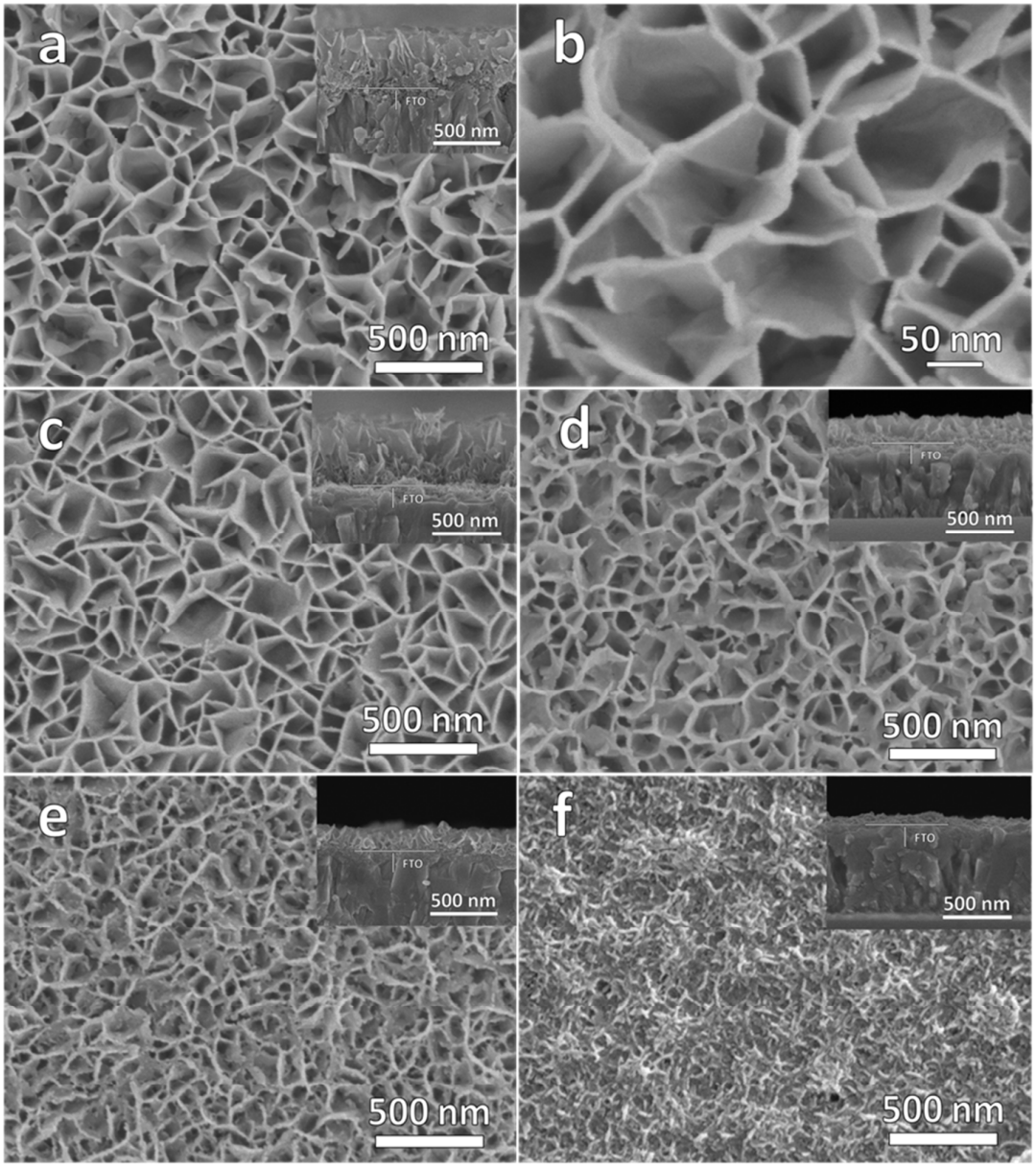

Fig. 3

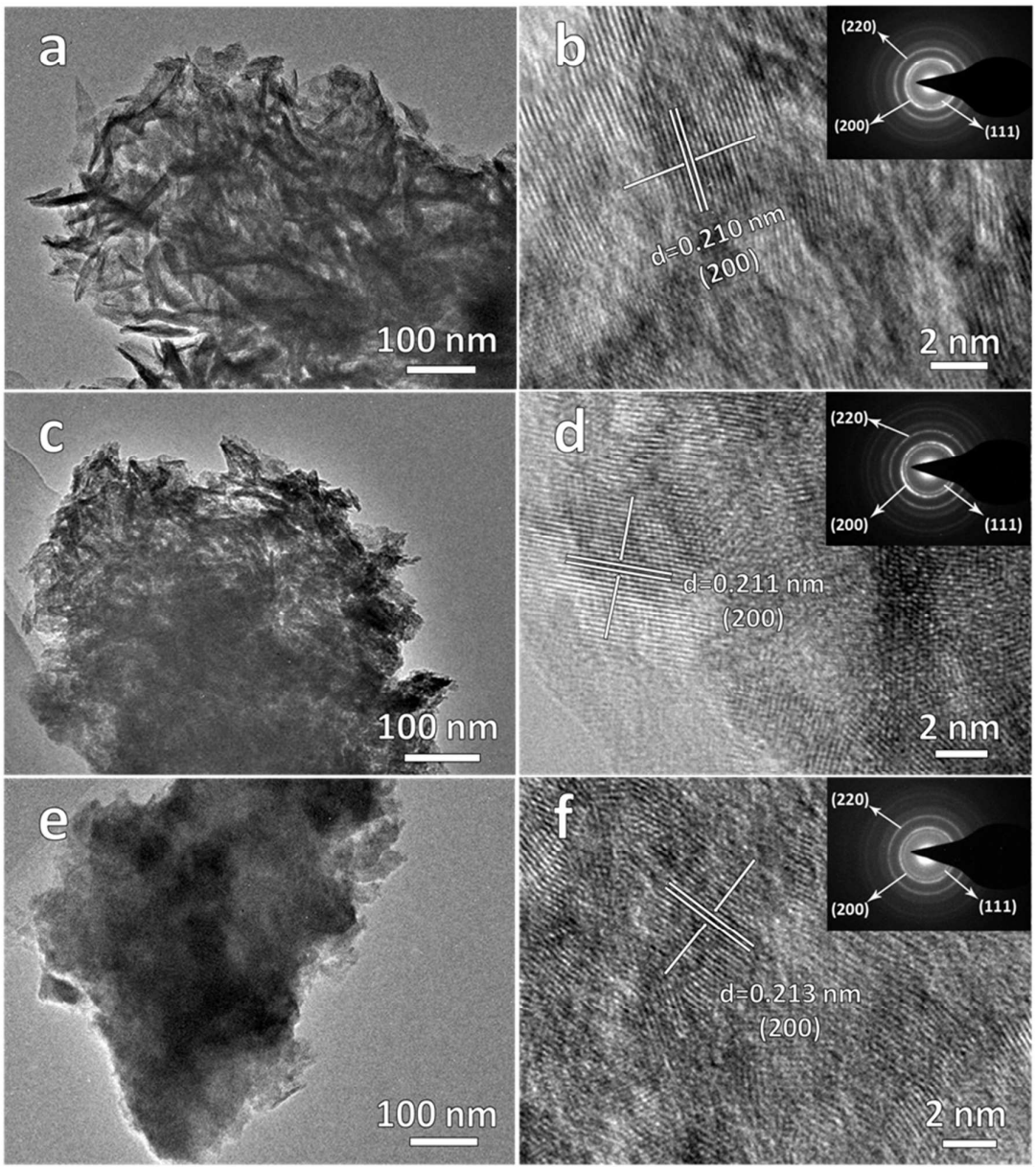

Fig. 4

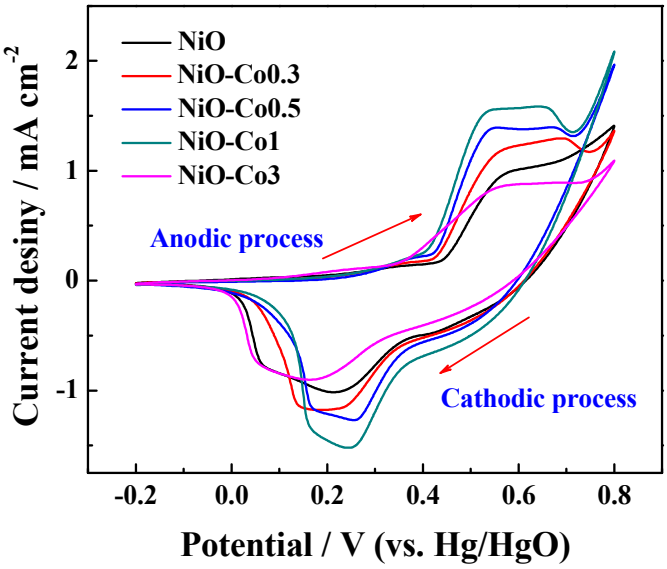

Fig. 5

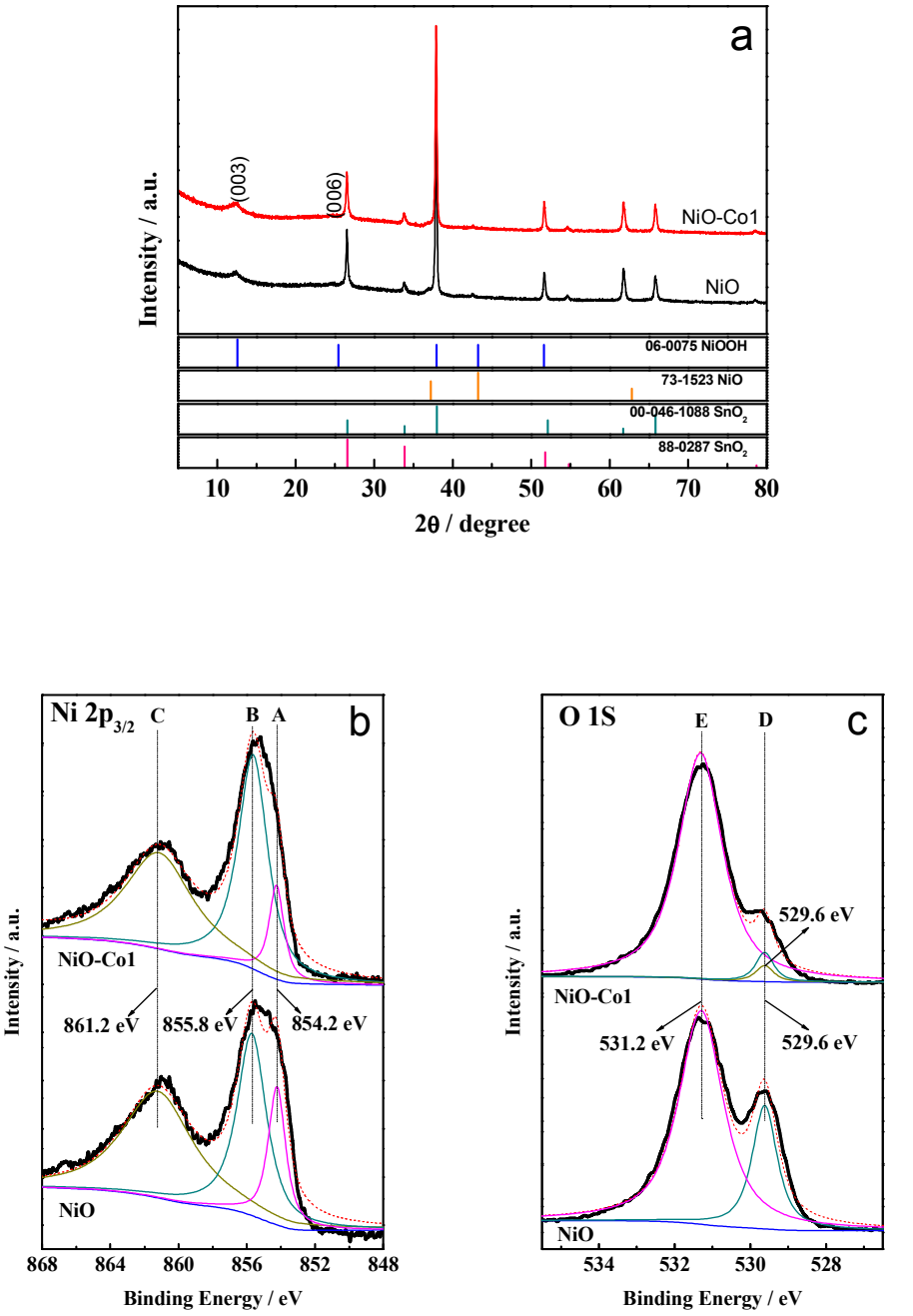

Fig. 6

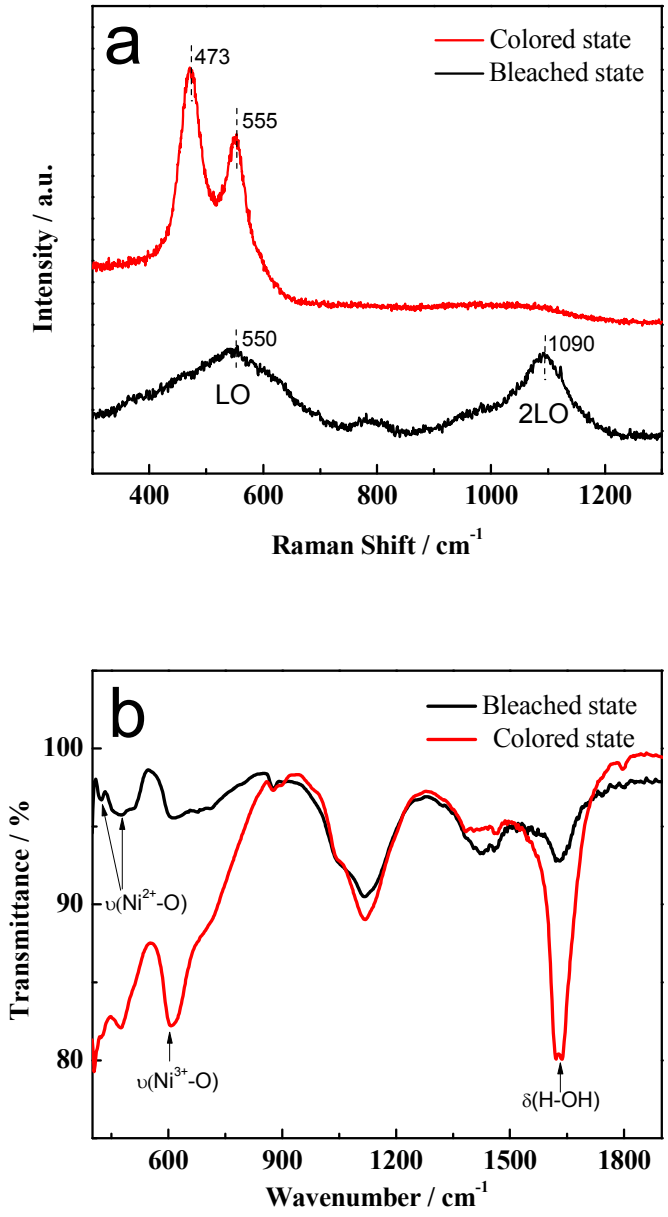

Fig. 7

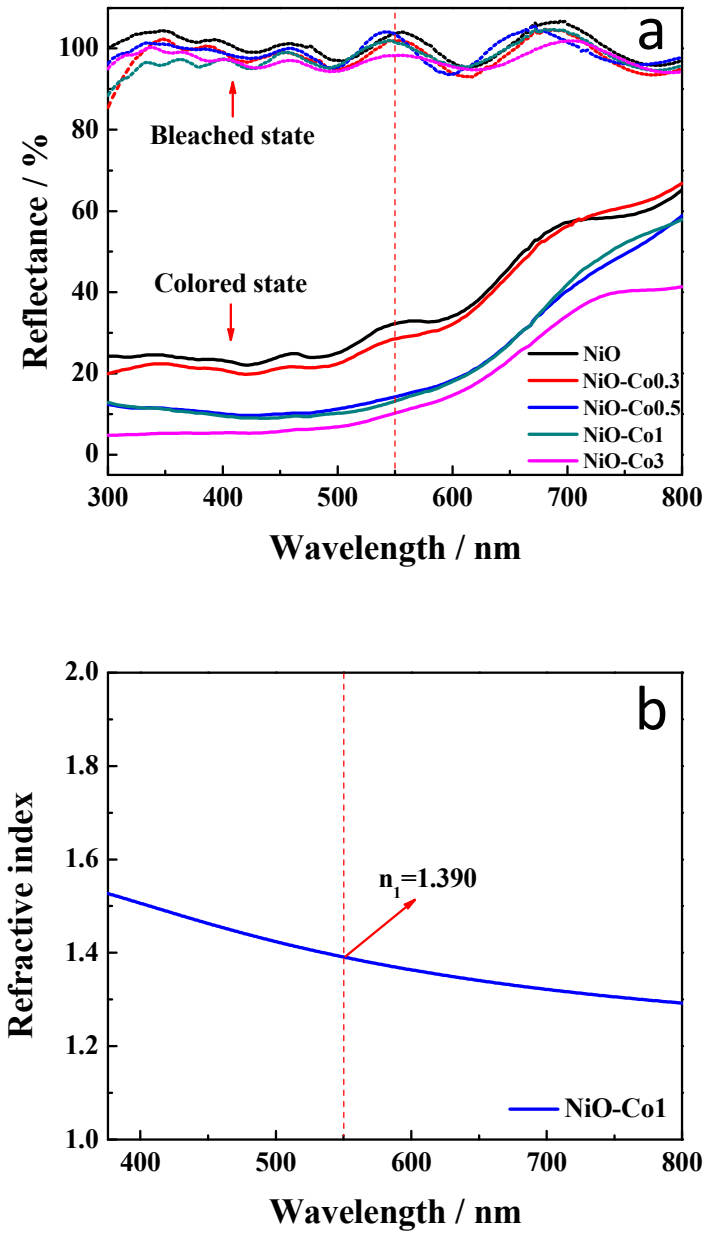

Fig. 8

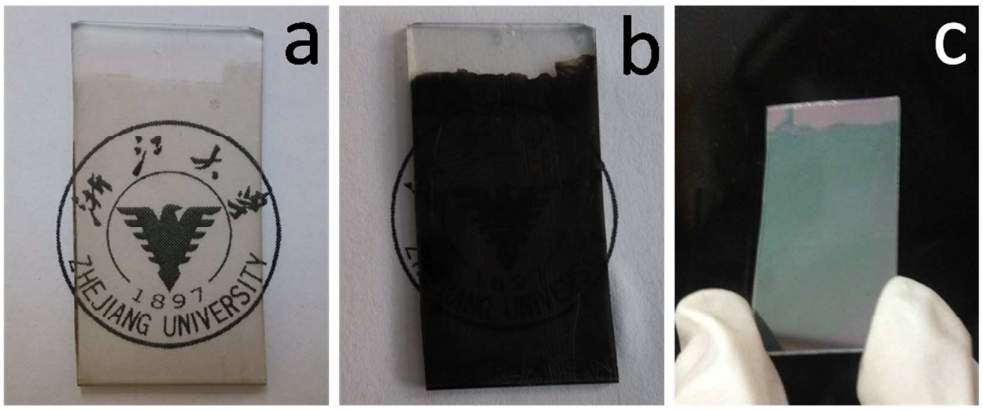

Fig.9

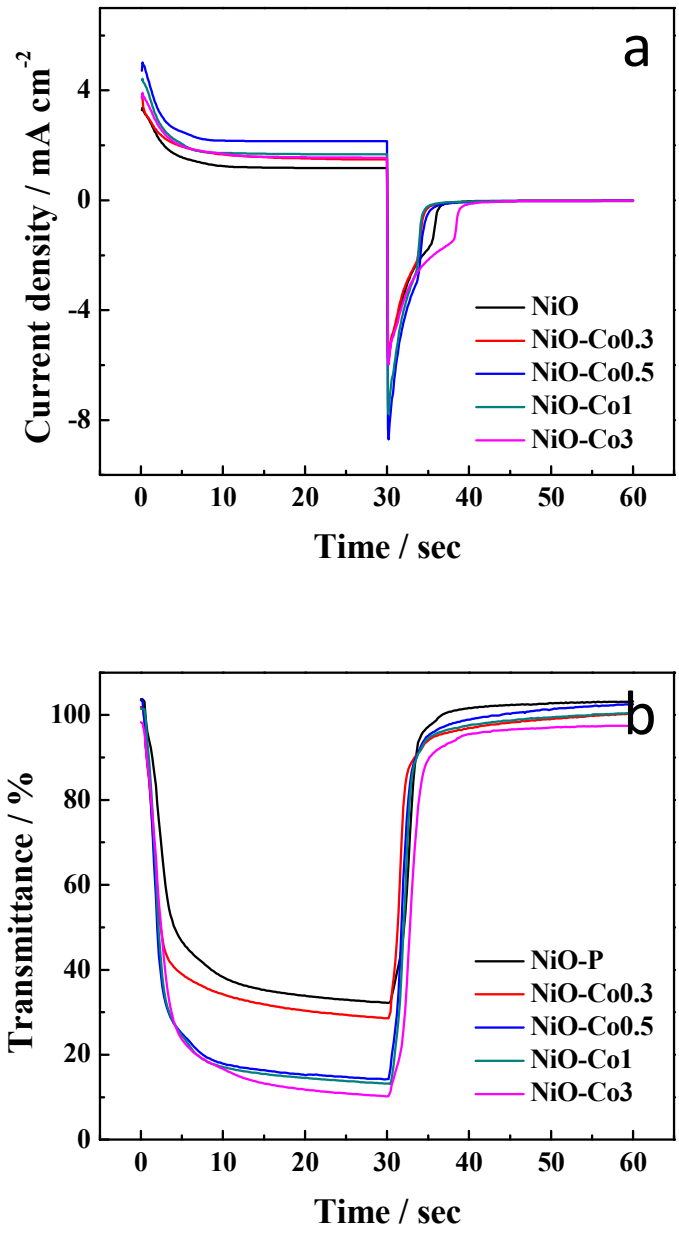

Fig. 10

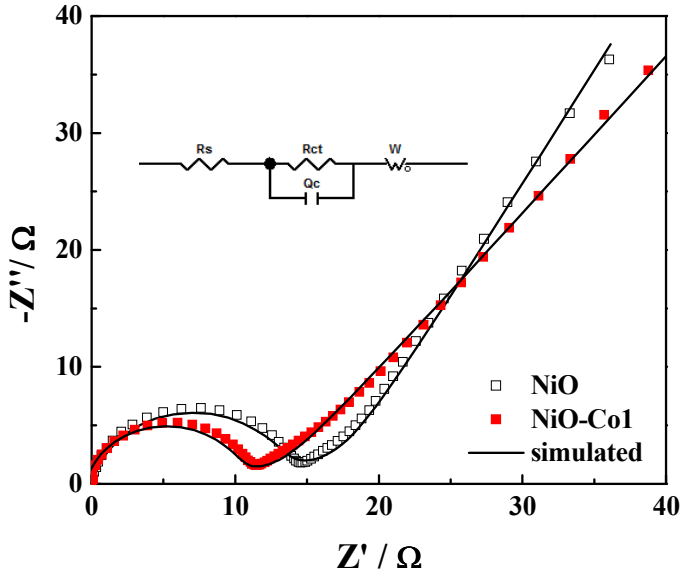

Fig. 11

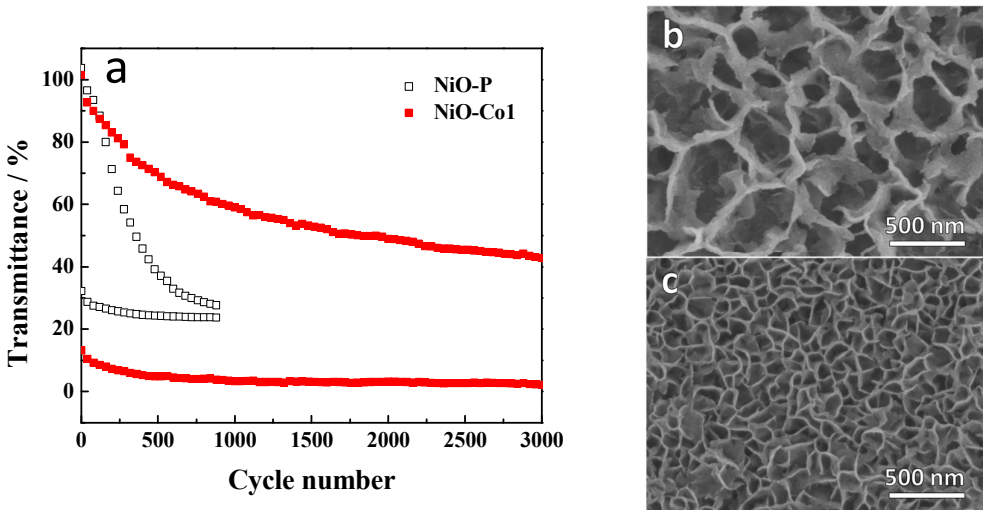

Fig. 12

Table of Content

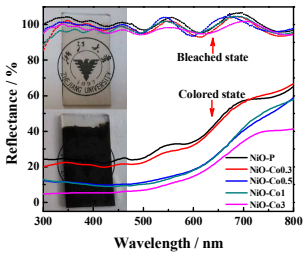

Co-doped NiO nanoflake array films with antireflective ability are fabricated by chemical bath deposition，exhibiting improved electrochromic performances.